IMECE2012-86926

MODELING OF MULTIFUNCTIONAL POROUS TISSUE SCAFFOLDS WITH CONTINUOUS DEPOSITION PATH PLAN

AKM B. Khoda
Department of Industrial Engineering
University at Buffalo
Buffalo, NY   14260, USA

Ibrahim T. Ozbolat
Department of Mechanical and Industrial Engineering
Center for Computer Aided Design
The University of Iowa
Iowa City, IA 52242-1527, USA

Bahattin Koc
Department of Industrial Engineering
University at Buffalo, Buffalo, NY, USA
&
Faculty of Engineering and Natural Sciences
Sabanci University, Istanbul 34956, Turkey
bkoc@buffalo.edu

ABSTRACT

A novel modeling technique for porous tissue scaffolds with targeting the functionally gradient variational porosity with continuous material deposition planning has been proposed. To vary the porosity of the designed scaffold functionally, medial axis transformation is used. The medial axis of each layers of the scaffold is calculated and used as an internal feature. The medial axis is then used connected to the outer contour using an optimum matching. The desired pore size and hence the porosity have been achieved by discretizing the sub-regions along its peripheral direction based on the pore size while meeting the tissue scaffold design constraints. This would ensure the truly porous nature of the structure in every direction as well as controllable porosity with interconnected pores. Thus the desired controlled variational porosity along the scaffold architecture has been achieved with the combination of two geometrically oriented consecutive layers. A continuous, interconnected and optimized tool-path has been generated for successive layers for additive-manufacturing or solid free form fabrication process. The proposed methodology has been computationally implemented with illustrative examples. Furthermore, the designed example scaffolds with the desired pore size and porosity has been fabricated with an extrusion based bio-fabrication process.

Keywords: Medial axis, variational porosity, internal scaffold architecture.

1   INTRODUCTION

To stimulate the guided tissue regeneration and expediting the tissue regeneration, the researchers tried to use porous structure conduits to deliver bio-molecules (usually cytokines) and/or cells to the tissue area. One major purpose for using such porous structures is to induce amenable bio-reactor in the tissue regeneration site and protect the seeded cell/ bio-molecules against host immunorejection [1] and thus stimulating the regeneration process. Even though the internal architecture of scaffolds may have significant influence on the cellular microenvironment, but few researches have focused on the designing internal architecture of the porous structure and even fewer have tried to optimize its geometry. The rationale for this might be that with the most commonly used traditional scaffold fabrication processes, it is often difficult to produce functional structures with pre-defined morphology. Moreover controllable uniformity, repeatability and/or distribution of material and internal architecture are extremely difficult to achieve in such processes.

Micro-fabrication and bio-microelectromechanical system (bio-MEMS) technology has become an attractive tool for developing tissue-engineering systems because of the improved spatial resolutions over traditional polymeric fabrication techniques [2, 3]. Especially the development of 3D printing or Solid Free Form (SFF) techniques and the improvement in biomaterial's properties by synergy provides the leverage of using SFF techniques to fabricate interconnected porous structures. As a result, SFF techniques are considered to be a

viable alternative for controlling the scaffold architecture. A number of researchers have successfully used various SFF techniques along with a wide range of bio-materials to fabricate the scaffolds. A comprehensive review on bio-fabrication of scaffolds using SFF processes can be found in [4-6]. Despite such a unique freedom to fabricate complex design geometries, the SFF are mainly used to fabricate scaffold structures with uniform porosity. But the scaffolds with uniform porosity do not capture the spatial properties required for the replaced tissue and are not capable of capturing the design of the replaced tissue bio-mimetically [7, 8]. The desired choreographed multi-functionality of such structures may only be achieved with optimally designed variational porosity spatially [9, 10]. Thus the need for a reproducible and fabricatable structure design with controllable gradient in porosity is obvious but possibly limited by design and fabrication limitations [11, 12].

In this paper, we proposed a novel method to addresses the design limitations by designing functionally gradient variational porosity architecture that conforms the anatomical shape of the damage tissue and maintains the continuity with connectivity.

2 METHODOLOGY

To design a tissue scaffold, the 3D geometry of the targeted damaged area needs to be extracted. Firstly, medical image obtained from Computed Tomography (CT) or Magnetic Resonance Imaging (MRI) is used to get the geometric and topology information of the replaced tissue. The three dimensional geometric model is then sliced by a set of intersecting planes parallel to each other to find the layer contours which are suitable for additive manufacturing processes. All contour curves are simple planner closed curves and the general equation for these contour can be parametrically represent as:

$$C_i(t_i) = (x(t_i), y(t_i)) \qquad \forall i = 0,...m$$
$$t_i \in [a_i, b_i] \qquad (1)$$
$$C_i(a_i) = C_i(b_i)$$

Here, $C_i(t_i)$ represent the parametric equation for i^{th} contour with respect to parameter t_i at a range between $[a_i, b_i]$.

2.1 Medial axis

To vary the porosity of the designed scaffold based on the required functionality, we introduce medial axis (MA) for each of the contour C_i as an geometric internal feature [13]. The medial axis is the topological skeleton of a closed contour which is also a symmetric bisector. MA can be used as base for varying the porosity. Moreover, characteristics such as uniqueness, invertibility and topological equivalence make the medial axis a suitable candidate for the internal feature.

A medial-axis, $M_i(C_i)$ in this paper has been generated for every contour or slice C_i using offsetting as shown in Fig 1(a).

The approximated offset curve $C_i^d(t_i)$ of the contour curve $C_i(t_i)$ at a distance d from the boundary is defined by:

$$C_i^d(t_i) = C_i(t_i) + d\vec{N}(t_i) \qquad (2)$$

Where $\vec{N}(t_i)$ is the unit normal vector on curve $C_i(t_i)$ at a parametric location t_i. Such offset may generate self-intersection if d is larger than minimum radius of curvature at any parametric location t_i of the offset curve $C_i^d(t_i)$. Any self-intersections during offsetting has been eliminated by implementing the methodology discussed in our earlier work [11]. A singular point is obtained at each self-intersection event where there is no C^1 continuity. Also any branch point for medial axis in this paper is assumed to be located at the center of loci that is tangent to three boundaries simultaneously and the brunch connection has been determined higher offset resolution and interpolation as discussed in Ozbolat et al [14]. The medial axis has been obtained by connecting the loci together as piece wise linear curve.
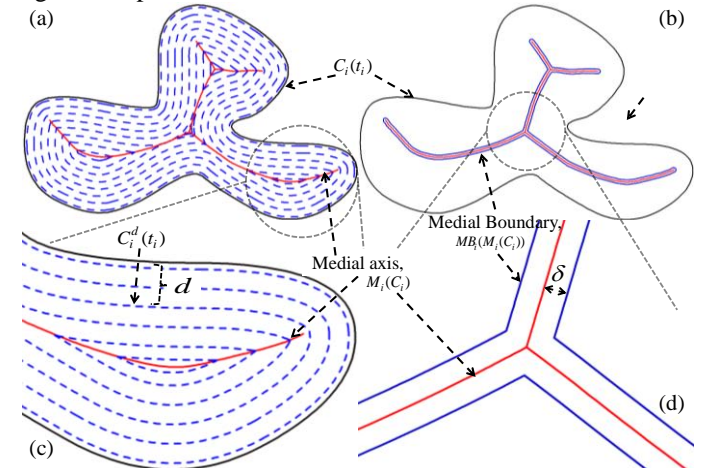

Fig. 1: (a) The medial axis generation, (b) medial boundary, (c) and (d) corresponding zoomed view.

2.2 Ruling lines between features

The scaffold area needs to be divided with finite number of segment by drawing line between the slice contour C_i and its corresponding medial axis MA, $M_i(C_i)$. To avoid non-manifold surface generation, a feature matching ruling lines generation technique [3] has been implemented by solving a dynamic programming. For the ease of calculation and proper implementation of the methodology, a medial region has been constructed from the medial axis. The medial region has been defined as the sweeping area covered by a circle whose loci of centers are the constructed medial axis. A medial region boundary, $MB_i(M_i(C_i))$ curve is constructed by offsetting medial axis (MA) in both inward and outward directions with a distance $\delta : ll' \leq 2\delta \leq ul'$ where ul' and ll' represent upper and lower width for biologically allowable pore size for cell in growth as shown in Fig 1(b). The width of this medial boundary channel δ can be higher if the scaffold is targeted for perfusion

bioreactor cell culture [15] which could be important methodology for reducing cell morbidity with proper nutrient and oxygen circulation. Any self intersection points or loops of the offset curve is then removed via the same methodology discussed earlier [11] and a closed, planner medial boundary has been achieved.

Both the contour curve $C_i(t_i)$ and medial boundary, $MB_i(M_i(C_i))$ curve are closed, planner and non-self intersecting in nature and are parametrically divided into n_1 and n_2 independent finite number of sections with a set of points $P_{C_i} = \{p_{c_i,j}\}_{j=0,1..n_1}$ and $P_{MB_i} = \{p_{MB_i,k}\}_{k=0,1.n_2}$ respectively; Where $p_{c_i,j} = C_i(t_{i,j})$ and $t_{i,j} = [t_{i,0}, t_{i,n_1}]$ and similarly $p_{MB_i,k} = MB_i(t_{i,k})$ and $t_{i,k} = [t_{i,0}, t_{i,n_2}]$. The dynamic programming applies distance based optimization between the features point set $\|P_{C_i} P_{MB_i}\|$ for matching with singularity and connecting the ruling lines. Both over connectivity and zero-connectivity with those point set are addressed with the same methodology discussed in our earlier paper [3]. Thus the methodology would generate at least n number of uninterrupted ruling lines, $RL = \{rl_n\}_{n=\max\{n_1,n_2\}}$ between contour curve and medial boundary and are act as resolution for the process.
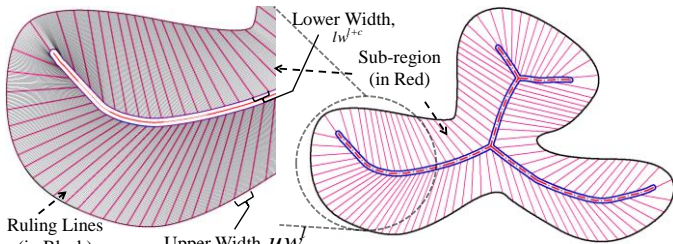

Fig. 2: Sub-region formation from ruling lines.

2.3 Sub-regions accumulation

The scaffold area has been segmented into equal area sub-regions by accumulating the area between ruling lines as shown in Fig 2. Such sub-regions can be considered as channel between the contour and the medial boundary which is the deepest region. It must also satisfy the biological requirement i.e. nutrient, fluid and oxygen flow. Thus the sub-region accumulation has been considered as an optimization problem with constraint that ensures functional requirement and uniformity. The following minimization problem [3] has been solved to achieve the set of sub-regions, $S = \{s_l\}_{l=0,1...L}$ where l is the number of feasible sub-regions.

$$\text{Min} \quad \sum_l (S_0^{Area} - S_l^{area}) \quad \forall \ l \tag{3}$$

Subject to-

$$ll \le lw^j \le ul \quad \forall \ l \tag{4}$$

$$ll \le uw^j \le ul \quad \forall \ l \tag{5}$$

$$\sum_l S_l^{area} \approx \dot{A} \tag{6}$$

$$S_m \cap S_n = \varnothing \ \forall \ m \text{ and } n = 0..l \tag{7}$$

Here, S_0^{area} is user-defined excepted sub-region area which is a constant, S_l^{area} is the lth sub-region area, lw^j is the lower width and uw^j is the upper width after accumulation, $\dot{A}$ is the total scaffold area. ul and ll represent the upper and lower limit for allowable sub-region width that satisfy the bio-logical requirement and the values are based on the design objective and available fabrication system used for fabrication. In literature [16, 17] the range for lower width has been suggested 100 μm - 350 μm for hard tissue and 30 μm - 150 μm for soft tissue. For upper width even a wider range of 200 μm - 900 μm has been suggested.

2.4 Decomposing the sub-region's base

The generated sub-regions are multi-directional in nature and their alignment depends upon the outer contour profile and ruling line density. Moreover, the sub-regions are constructed in a way so that they share arms with the adjacent neighboring sub-region. So, each sub-region is basically separated from its adjacent neighbor by the sub-region's arm which itself is a ruling line as, $SA = \{SA_l\}_{l=0,1,..L}$ where $SA \subseteq RL$. Thus the generated sub-region set can be represented with the two end points, $SP = \{sp_l\}_{l=0,1..L}$ and $BP = \{bp_l\}_{l=0,1..L}$ of the corresponding arm where, sp_l and bp_l are the starting points and base points of lth sub-region as shown in Fig. 3.
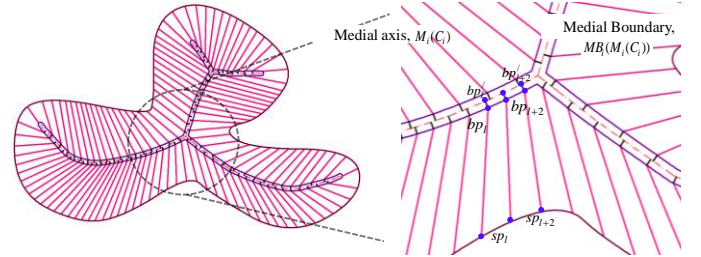

Fig. 3: Decomposing of sub-region base on medial axis.

The sub-regions arm set SA are cut through by the medial boundary which makes the medial region a long channel. To ensure the structural integrity along the medial region and the overall scaffold architecture, the point set BP for all sub-regions need to be projected on the medial axis along the direction $\overrightarrow{N_l}(bp_l)$ which would create a new point set $BP^/ = \{bp_l^/\}_{l=0,1..L}$. Here, $\overrightarrow{N_l}(bp_l)$ is the unit normal vector on the medial boundary $MB(bp_l)$ at a parametric point location bp_l and $bp_l^/$ is the projected point location corresponding to bp_l as shown in Fig. 3. The projecting lines would divide the long medial region into smaller pore size ensuring both biological and mechanical functionality.

3

2.5 Pore cell generation

To generate the porosity in the scaffold each equal area sub-region has been considered and divided according to area across their arms shown in Fig. 4 (a). These segments of each sub-section can be considered as a pore cell, PC_l^m of the scaffold which is the mth pore cell area of lth sub-region and $m = 0,1,....,M$ is the number of pore cell in any sub-region. Because of the free-form shape of the outer contour and the accumulation pattern, the generated sub-regions have highly anisotropic shapes which eventually generates anisotropic pore cell. The following algorithm has been used to divide the sub-regions.

$$\text{Min} \quad \sum_{m=0}^{M} \left| PC(m) - PC_l^m \right| \quad \forall \quad 0 \le l \le L \quad (8)$$

Subject to-

$$\frac{S_0^{area}}{\max\_PC} \le M \le \frac{S_0^{area}}{\min\_PC} \quad (9)$$

$$\sum_{m=0}^{M} PC_l^m = S_l^{area} \quad \forall \quad 0 \le l \le L \quad (10)$$

$$PC_x^m = PC_y^m \quad \forall \quad 0 \le m \le M, \ 0 \le x, y \le L \quad (11)$$

This minimization problem us used to reduce the deviation from the desired or expected pore cell area, $PC(m)$ with the generated pore cell area, PC_l^m. $\max\_PC$ and $\min\_PC$ denotes the maximum and minimum allowable pore cell area respectively. In literature, the designed pore cells are usually uniform shape, but because of the anisotropy the allowable pore cell area range needs to be interpreted and discussed in Khoda et.al.[3]. The total number of pore cell in every single sub-regions need to be the same to ensure fabrication continuity as represented in Equation (10).
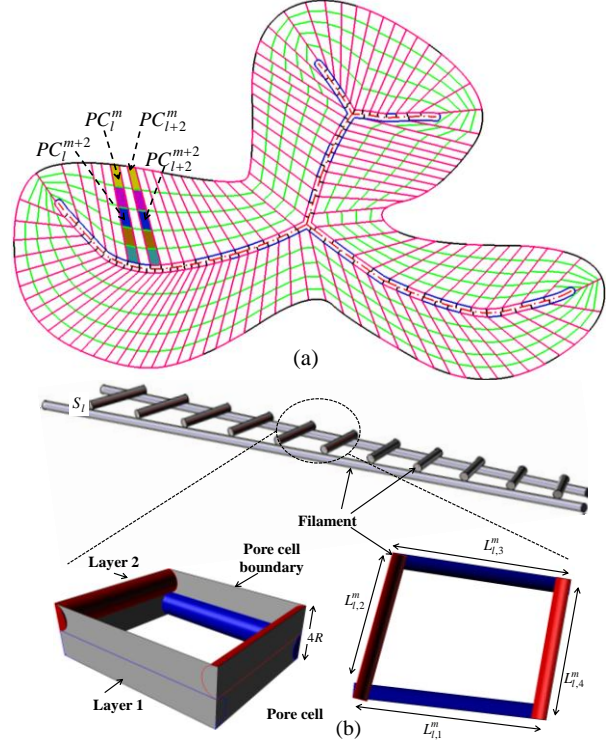
Fig. 4: (a) Dividing the sub-regions to generate pore cell (b) porosity calculation for anisotropic pore cell.

The porosity for the generated anisotropic pore cell can be measured by the following equation [3]:

$$\%Porosity_l^m = 1 - \frac{(L_{l,1}^m + L_{l,2}^m + L_{l,3}^m + L_{l,4}^m) \times \pi \times R^2}{Area\_L_{l,1}^m L_{l,2}^m L_{l,3}^m L_{l,4}^m \times 8 \times R} \quad \forall \ l, m \ (12)$$

Where, R is the radius of the filament, $\%Porosity_l^m$ is the porosity of mth pore cell area in l^{th} sub-region and $L_{l,1}^m, L_{l,2}^m, L_{l,3}^m, L_{l,4}^m$ are the four arms of pore cell as shown in Fig. 4(b).

2.6 Tool path Planning

The proposed bi-layer stack pore design represents the controllable and desired gradient in porosity along the scaffold architecture. Even though some earlier research emphasis on the variational porosity design but fabrication procedure with existing fabrication technique remain a challenge for those designs [18]. In this work, a continuous deposition path planning method to fabricate the bi-layer model with SFF technique has been proposed which ensure connectivity of internal channels' network.

To ensure the continuity throughout the sub-regions layer, the deposition path has been planned through the generated sub-region's arm SA and bridge the medial region via the projected points $bp_l^/$ on the medial axis. Based on the location of the corresponding $bp_l^/$ point, a distance based consecutive point search algorithm [13] has been used to ensure

the connected tool-path progression. Moreover, during the crosshatching through the medial region, the points set $BP^{/}$ has been reevaluated and eliminated as

$$BP^{/} = BP^{/} \bigcap bp_c^{/}, bp_b^{/} : \left| bp_c^{/} bp_b^{/} \right| \leq \delta / 2 \quad \forall \ bp_c^{/} \text{ and } bp_b^{/} \in BP^{/}$$

and such eliminating would increase the continuity during deposition. Fig. 5 shows the tool-path for the sub-region layer.
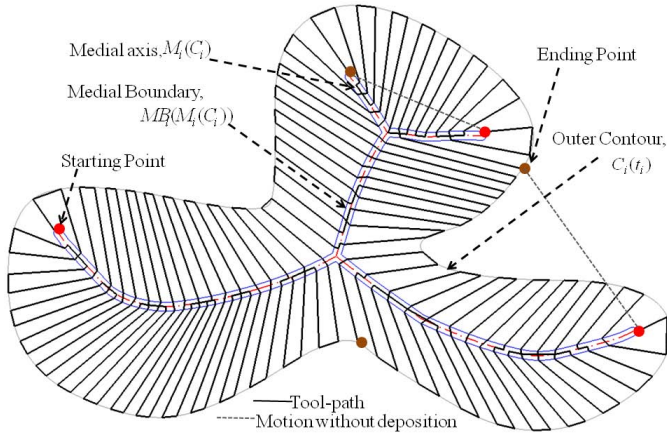
Fig. 5: Simulation of tool-path for the deposition through Sub-region's arm.

For the second layer, the proposed tool-path has been generated through the pore cell generating lines that passes across the sub-regions. But because of the irregular geometry, these lines rarely have coherent connection between them as shown in Fig. 4(a). Connecting those lines consecutively without any transformation would generate stepped dominated polygon path which might not be favorable for SFF system [3]. For smoothing this stepped dominated spiral path, an area weight based point insertion algorithm [3], has been implemented and shown in Fig. 6(a). Finally after generating the deposition path for both layer individually, they are combined together to make the continuous and interconnected tool path as shown in Fig. 6(b).
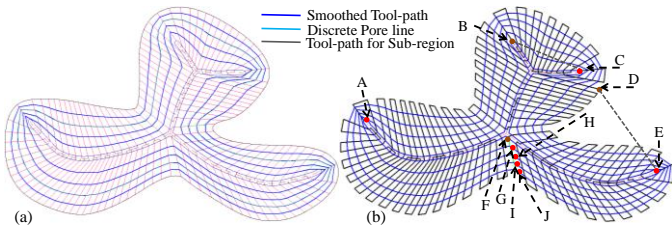

Fig. 6: (a) Smoothed pore generating tool-path (b) Final combined tool-path with start-ending sequence as A-B-C-D-E-F-G-H-I-J.

3   IMPLEMENTATION

The proposed techniques have been implemented with a 2.3 GHz PCs using Rhino Script and Visual Basic programming languages on a femur head slice extracted using ITK-Snap 1.6 [19] and Mimics Software[20]. The following femur slice (shown in Fig. 7) has been used to implement the methodology targeting the variable but controllable porosity along its

architecture with 50%-60%-70%-80%-90%-75%-60%-50% porosity from outer to inner region and 150 micron filament diameter. Fig. 7 shows the generated medial axis and the corresponding medial boundary for the example. The scaffold area has been discretized with 225 numbers of sub-regions accumulated from 2620 number of ruling line generated by the methodology described in section 2.2. Sub-regions are divided to generate pore cell according to the area interpretation of the corresponding porosity as shown in Fig. 8(b).
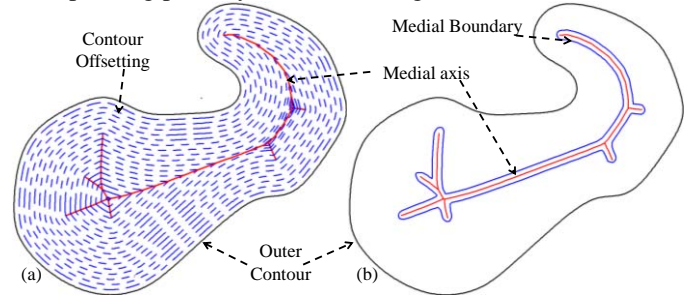

**Fig. 7**: (a) The medial axis (b) medial boundary formation.
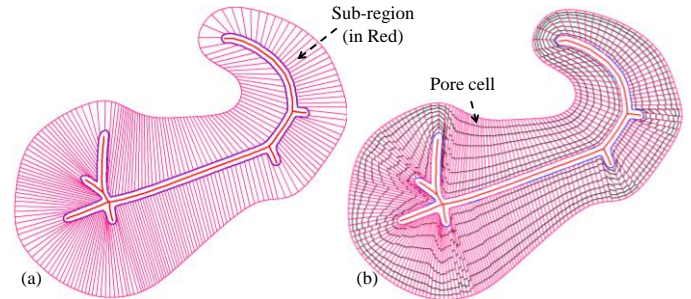
Fig. 8: (a) Sub-regions formation from the ruling lines (b) dividing sub-regions by generating desired area pore cell.

To ensure the fabricatability of the designed scaffold architecture, the lower widths of the sub-regions are decomposed on the medial axis with the methodology discussed in section 2.4. Thus by crosshatching the sub-region's arm through the medial region, the continuity has been achieved as shown in Fig. 9(b). Tool-path for the pore cell generating layer has been done by a smoothing algorithm discussed earlier and the combined layer has been shown in Fig. 10(a).
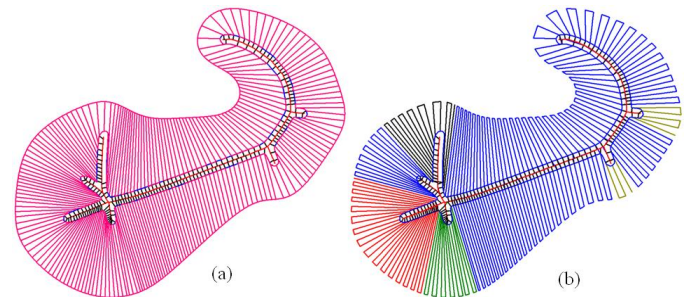
Fig. 9: (a) Decomposing of sub-region base on medial axis (b) Tool-path for the deposition through Sub-region's arm (color represent different segment of the tool-path).

Copyright © 2012 by ASME
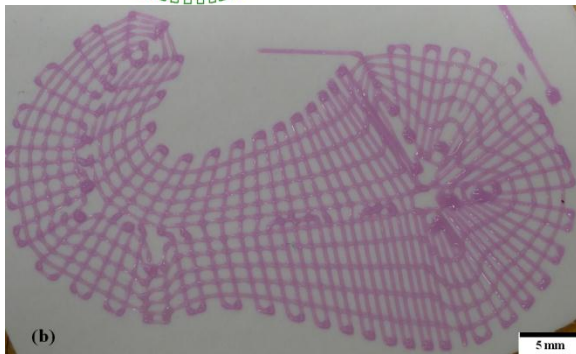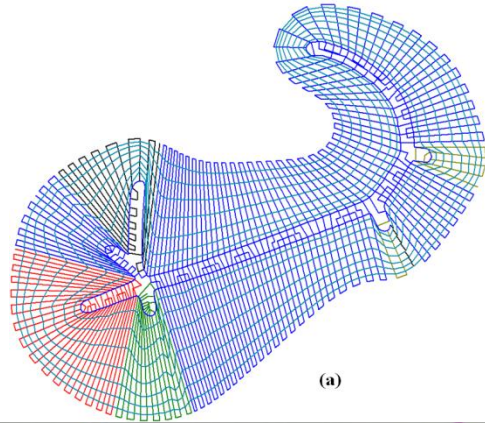
Fig. 10: (a) Final combined tool-path for controllable porosity along its architecture with 50%-60%-70%-80%-90%-75%-60%-50% porous from outer to inner region (b) bio-fabrication of two consecutive for the femur slices with a constant porosity of 75%.

For demonstration purpose, two consecutive slices of the femur example was fabricated with a 3D micro-nozzle biomaterial deposition system [3]. To fit into the working envelope of the fabrication system, the actual human femur model has been scaled down by 33%. In the fabricated model, a total of 103 sub-regions have been used to discretize the scaffold area. Each sub-region has been segmented with five equal area pore cells as shown in Fig. 10 (b). The model has been fabricated with 250 micrometer substrate diameter. As shown in Figure 10(b), there are some material over-depositions along the outer and inner edges. This is due to the sharp and sudden changes in the tool-path direction along the edge. Speeding up the process particularly along the edge could alleviate this over deposition but complete elimination would be a challenge for our current fabrication setup.

4   CONCLUSION

We propose the design for controllable porosity with desired gradient along the scaffold architecture. The design methodology ensures the fabricatability of the design by considering the extrusion based SFF techniques. The scaffold area has been discretized with sub-regions and then is divided into pore cell to achieve the desired porosity. To ensure the proper interpretation of the design objective during its fabrication, a feasible tool-path plan has been proposed which would minimize the deviation between design and actual structure. The proposed methodology generates interconnected and controlled pore size with desired accuracy along the scaffold architecture resulting controllable variational porosity with a continuous deposition path planning appropriate for SFF processes. Even though the final porosity might deviate from the designed porosity due to the anisotropic nature of the generated pore cell, but this error can be minimized and controlled along the scaffold structure. Controlling the pore cell and its porosity could be the future direction for this research.

REFERENCES

[1] Levenberg, S., and Langer, R., 2004, "Advances in Tissue Engineering," Current Topics in Developmental Biology, P. S. Gerald, ed., Academic Press, pp. 113-134.
[2] Bettinger, C. J., Weinberg, E. J., Kulig, K. M., Vacanti, J. P., Wang, Y., Borenstein, J. T., and Langer, R., 2006, "Three-Dimensional Microfluidic Tissue-Engineering Scaffolds Using a Flexible Biodegradable Polymer," Advanced Materials, 18(2), pp. 165-169.
[3] Khoda, A., Ozbolat, I. T., and Koc, B., 2011, "A functionally gradient variational porosity architecture for hollowed scaffolds fabrication," Biofabrication, 3(3), pp. 1-15.
[4] Yeong, W.-Y., Chua, C.-K., Leong, K.-F., and Chandrasekaran, M., 2004, "Rapid prototyping in tissue engineering: challenges and potential," Trends in Biotechnology, 22(12), pp. 643-652.
[5] Hutmacher, D. W., Sittinger, M., and Risbud, M. V., 2004, "Scaffold-based tissue engineering: rationale for computer-aided design and solid free-form fabrication systems," Trends in Biotechnology, 22(7), pp. 354-362.
[6] Gomez, C., 2007, "A Unit Cell Based Multi-scale Modeling and Design Approach for Tissue Engineered Scaffolds," Drexel University
[7] Butscher, A., Bohner, M., Hofmann, S., Gauckler, L., and Müller, R., 2011, "Structural and material approaches to bone tissue engineering in powder-based three-dimensional printing," Acta Biomaterialia, 7(3), pp. 907-920.
[8] Khoda, A., and Koc, B., 2012, "Designing Controllable Porosity for Multi-Functional Deformable Tissue Scaffolds," ASME Transactions, Journal of Medical Device (In Press).
[9] Adachi, T., Osako, Y., Tanaka, M., Hojo, M., and Hollister, S. J., 2006, "Framework for optimal design of porous scaffold microstructure by computational simulation of bone regeneration," Biomaterials, 27(21), pp. 3964-3972.
[10] Lin, C. Y., Kikuchi, N., and Hollister, S. J., 2003, "A Novel Method for Biomaterial Internal Architecture design to match bone plastic properties with desired porosity," Journal of Biomechanics, 37, pp. 623–636.
[11] Khoda, A. K. M. B., Ozbolat, I. T., and Koc, B., 2011, "Engineered Tissue Scaffolds With Variational Porous Architecture," Journal of Biomechanical Engineering, 133(1), p. 011001.
[12] Sobral, J. M., Caridade, S. G., Sousa, R. A., Mano, J. F., and Reis, R. L., 2011, "Three-dimensional plotted scaffolds

with controlled pore size gradients: Effect of scaffold geometry on mechanical performance and cell seeding efficiency," Acta Biomaterialia, 7(3), pp. 1009-1018.

[13] Khoda, A., Ozbolat, I. T., and Koc, B., 2012, " Modeling of Variational Gradient Porous Architecture with Multi-directional Filament Deposition in 3D Scaffolds," Journal of Computer Aided Design and Applications (In Press).

[14] Ozbolat, I. T., and Koc, B., 2011, "Multi-directional blending for heterogeneous objects," Computer-Aided Design, 43(8), pp. 863-875.

[15] Gaetani, R., Doevendans, P. A., Metz, C. H. G., Alblas, J., Messina, E., Giacomello, A., and Sluijter, J. P. G., "Cardiac tissue engineering using tissue printing technology and human cardiac progenitor cells," Biomaterials(0).

[16] Karande, T. S., Ong, J. L., and Agrawal, C. M., 2004, "Diffusion in Musculoskeletal Tissue Engineering Scaffolds: Design Issues Related to Porosity, Permeability, Architecture, and Nutrient Mixing," Annals of Biomedical Engineering, 32(12), pp. 1728-1743.

[17] Hollister, S. J., Maddox, R. D., and Taboas, J. M., 2002, "Optimal design and fabrication of scaffolds to mimic tissue properties and satisfy biological constraints," Biomaterials, 23(20), pp. 4095-4103.

[18] Khoda, A. B., and Koc, B., 2011, "Designing Functional Porosity in Heterogeneous Bone Tissue Scaffolds with Variational Filament Modeling," CAD (Submitted).

[19] www.itksnap.org, 2008, "ITK-SNAP," 1.6.

[20] http://www.materialise.com/mimics, 2008, "Mimics."